1-17-2021

Nalfurafine Reduces Neuroinflammation and Drives Remyelination in Models of CNS Demyelinating Disease

Lisa Denny
Victoria University of Wellington, New Zealand

Afnan Al Abadey
Victoria University of Wellington, New Zealand

Katharina Robichon
Victoria University of Wellington, New Zealand

Nikki Templeton
Victoria University of Wellington, New Zealand

See next page for additional authors

Nalfurafine Reduces Neuroinflammation and Drives Remyelination in Models of CNS Demyelinating Disease

Authors

Lisa Denny, Afnan Al Abadey, Katharina Robichon, Nikki Templeton, Thomas E. Prisinzano, Bronwyn M. Kivell, and Anne C. La Flamme

ORIGINAL ARTICLE

Nalfurafine reduces neuroinflammation and drives remyelination in models of CNS demyelinating disease

Lisa Denny[1,2], Afnan Al Abadey[1,2], Katharina Robichon[1,2], Nikki Templeton[1,2], Thomas E Prisinzano[3] (iD), Bronwyn M Kivell[1,2†] (iD) & Anne C La Flamme[1,2,4†] (iD)

[1]School of Biological Sciences, Victoria University of Wellington, Wellington, New Zealand
[2]Centre for Biodiscovery, Victoria University of Wellington, Wellington, New Zealand
[3]Department of Pharmaceutical Sciences, University of Kentucky, Lexington, KY 40536, USA
[4]Malaghan Institute of Medical Research, Wellington, New Zealand

Correspondence

AC La Flamme, School of Biological Sciences,
Victoria University of Wellington,
PO Box 600, Wellington 6140, New Zealand.
E-mail: anne.laflamme@vuw.ac.nz

[†]Equal contributors.

Abstract

Objectives. Multiple sclerosis (MS) is a neurodegenerative disease characterised by inflammation and damage to the myelin sheath, resulting in physical and cognitive disability. There is currently no cure for MS, and finding effective treatments to prevent disease progression has been challenging. Recent evidence suggests that activating kappa opioid receptors (KOR) has a beneficial effect on the progression of MS. Although many KOR agonists like U50,488 are not suitable for clinical use because of a poor side-effect profile, nalfurafine is a potent, clinically used KOR agonist with a favorable side-effect profile. **Methods.** Using the experimental autoimmune encephalomyelitis (EAE) model, the effect of therapeutically administered nalfurafine or U50,488 on remyelination, CNS infiltration and peripheral immune responses were compared. Additionally, the cuprizone model was used to compare the effects on non-immune demyelination. **Results.** Nalfurafine enabled recovery and remyelination during EAE. Additionally, it was more effective than U50,488 and promoted disease reduction when administered after chronic demyelination. Blocking KOR with the antagonist, nor-BNI, impaired full recovery by nalfurafine, indicating that nalfurafine mediates recovery from EAE in a KOR-dependent fashion. Furthermore, nalfurafine treatment reduced CNS infiltration (especially CD4$^+$ and CD8$^+$ T cells) and promoted a more immunoregulatory environment by decreasing Th17 responses. Finally, nalfurafine was able to promote remyelination in the cuprizone demyelination model, supporting the direct effect on remyelination in the absence of peripheral immune cell invasion. **Conclusions.** Overall, our findings support the potential of nalfurafine to promote recovery and remyelination and highlight its promise for clinical use in MS.

Keywords: cuprizone, experimental autoimmune encephalomyelitis, kappa opioid receptor agonist, nalfurafine, neuroinflammation, remyelination, transmission electron microscopy, U50,488

INTRODUCTION

Multiple sclerosis (MS) is a neurodegenerative disease associated with chronic inflammation and demyelination in the central nervous system (CNS). It affects 2.5 million individuals worldwide and often leads to debilitating motor, sensory, autonomic and cognitive disabilities.[1] MS is considered an autoimmune disease involving the trafficking of pro-inflammatory CD4^{+} and CD8^{+} T cells into the CNS via the compromised blood–brain barrier (BBB), resulting in lymphocyte infiltration, microglia activation, focal inflammatory demyelination, and axonal damage by destroying the myelin sheaths formed by oligodendrocytes (OLs).[2,3]

There is currently no cure for MS, and the available immune-modifying medications are capable of reducing the relapse rate but are limited in their ability to halt disease progression and promote CNS repair. Hence, new therapies targeting different aspects of MS are highly sought after. Targeting the remyelination process has become a key area of interest in developing novel MS therapies. During the early phase of MS, remyelination can occur spontaneously within a month or two after active demyelination.[4] However, this spontaneous remyelination becomes sparse and limited to the borders of the lesions during the progressive stage of MS, as mature OLs fail to remyelinate.

The kappa opioid receptor (KOR) is expressed widely throughout both the human brain and spinal cord.[5–7] In the periphery, studies have found KORs in the rat GI tract, adrenal gland, kidney, lung, testis, ovary and uterus.[8,9] KOR expression has also been described on numerous immune cell populations.[10] Previous work has identified kappa opioid receptor agonism as a novel and clinically relevant therapy for enhancing oligodendrocyte progenitor cell (OPC) differentiation and remyelination. Du et al. (2016) revealed that KOR knockout mice exhibit a more severe disease phenotype in the experimental autoimmune encephalomyelitis (EAE) mouse model of MS, accompanied by significant demyelination and CNS infiltration, which indicates a role of endogenous KOR signalling for OL differentiation and myelination. Prophylactic administration of the traditional KOR agonist, U50,488, significantly reduced disease scores in EAE and also decreased demyelination and leukocyte infiltration into the spinal cord. U50,488

was also shown to enhance remyelination in the cuprizone-mediated demyelination model,[11] while Mei et al. (2016) found that U50,488 promoted OPC differentiation and wrapping in a developed micropillar array. Although these studies indicate that U50,488 is beneficial, it causes undesirable adverse effects including stress, dysphoria, aversion, anxiety, depression, impaired learning, and memory, all of which limit its clinical potential.[12,13] Hence, KOR agonism has the potential to be a very promising target in the treatment of MS for a KOR agonist with a favorable profile.

Nalfurafine is the only KOR agonist in clinical use and is significantly more potent than U50,488 in preclinical pain models.[14] In addition, nalfurafine is significantly more biased towards the G-protein pathway activation compared to U50,488 on both human and rodent KOR, with a lower potency for p38 activation, which is commonly associated with aversive side-effects.[15,16] Furthermore, long-term clinical trials and post-marketing surveillance involving intravenous or oral administration of nalfurafine have shown it to be well-tolerated in humans[17] and with fewer adverse effects in comparison to U50,488.[18] Here we investigated the ability of nalfurafine to reduce disease and promote remyelination in two animal models that recapitulate aspects of MS- EAE, and cuprizone intoxication.

RESULTS

Therapeutic treatment with nalfurafine enabled functional recovery from EAE

Previous studies investigating KOR agonists in EAE administered the agonists prior to the onset of disease. This could be viewed as a limitation, as the agonists could affect disease induction as well as progression. Using a more clinically relevant strategy, we investigated if nalfurafine was effective when administered therapeutically (i.e. upon the onset of EAE). We found that daily treatment with nalfurafine (0.1–0.0003 mg kg^{-1} intraperitoneally (i.p.) from disease onset (i.e. disease score ≥ 1.0) caused a significant reduction in disease burden when compared to vehicle-treated animals (Figure 1a; $P < 0.0001$). A 2-way ANOVA followed by the multiple comparisons test was used to compare the scores of each dose of nalfurafine to vehicle (Supplementary figure 2).

Therapeutic effects were most pronounced at the 0.03–0.01 mg kg^{-1} dose of nalfurafine, determined by significant and consistent recovery from 10 days post-treatment (dpt). Although nalfurafine did not alter peak disease (Supplementary figure 3a), all doses of nalfurafine reduced EAE-associated weight loss by the end of the experiment (45 days post-immunisation; d.p.i) compared to vehicle-treated mice (Supplementary figure 3b).

To specifically assess recovery from paralysis, animals were considered 'recovered' if they reached a disease score of 0.5 or below (i.e. no observable paralysis). Using this assessment, the majority (71%, 27/38) of nalfurafine-treated animals (0.01 mg kg^{-1}) fully recovered by day 23 post-treatment initiation (Figure 1b; $P < 0.0001$ compared to vehicle). In contrast, few vehicle-treated animals recovered (7.5%, 4/53). In addition, 0.01 mg kg^{-1} nalfurafine led to the greatest number of days in recovery (6.5 ± 0.97 mean ± SEM; $P < 0.0001$), whereas vehicle-treated animals spent few days in recovery (0.3 ± 0.14; Figure 1c). To access relapses, 'relapse' was defined by an increase in score by 1 full point from the lowest score of the remission after peak disease.[19] We found that compared to vehicle (0.49 ± 0.07), nalfurafine reduced the number of relapses per animal to day 23 post-treatment initiation (Figure 1d), with the greatest effect seen at the 0.01 mg kg^{-1} dose (0.07 ± 0.04; $P < 0.001$). Overall, these results suggest that therapeutic administration of nalfurafine is effective at promoting full recovery of EAE and reducing relapses. Nalfurafine at 0.01 mg kg^{-1} led to the most significant sustained recovery in EAE, as determined by a consistent recovery of disease scores and a dramatic reduction in relapse. Hence, this dose was used for all following experiments.

Nalfurafine was more effective than U50,488 at reducing disease

Since previous studies have shown that U50,488 significantly reduces disease in EAE, we evaluated whether nalfurafine at 0.01 mg kg^{-1} was similarly effective as U50,488. Although prior research administered U50,488 five days after immunisation (i.e. before disease onset), upon comparison with previously collated data, we found that therapeutic treatment of EAE animals with U50,488 (1.6 mg kg^{-1} i.p. daily) also caused a

significant reduction in disease compared to vehicle (Figure 1e; $P < 0.0001$). However, we found that nalfurafine (0.01 mg kg^{-1} i.p. daily) was more effective at reducing disease than U50,488 ($P < 0.05$). Moreover, U50,488 treatment had no effect on peak disease compared to the nalfurafine or vehicle groups (Supplementary figure 3c; $P < 0.01$). However, within these experiments, neither nalfurafine nor U50,488 ameliorated EAE-associated weight loss from the time of treatment initiation (indicated by the grey bar; 10–14 d.p.i) (Supplementary figure 3d). In addition, recovery was more frequent with nalfurafine compared to U50,488 (47%; 8/17; Figure 1f). Both nalfurafine and U50,488 significantly enhanced the number of days spent in recovery compared to vehicle (Figure 1g). However, although the mean recovery rate for nalfurafine-treated animals was greater than U50,488 (4.4 ± 1.6; $P < 0.01$), this did not reach significance ($P = 0.28$). Furthermore, U50,488 treatment improved disease recovery but failed to reduce relapses (0.66 ± 0.18) compared to vehicle (Figure 1h). Taken together, these results indicate that nalfurafine has a greater therapeutic effect than U50,488 in promoting disease recovery in EAE.

KOR activation was involved in nalfurafine-mediated recovery from EAE

To verify that amelioration of EAE by nalfurafine is KOR-dependent, the KOR was blocked with a highly selective and potent KOR antagonist, nor-BNI. Upon disease onset, animals were administered vehicle or nor-BNI (10 mg kg^{-1} i.p. weekly) and administered vehicle or nalfurafine (0.01 mg kg^{-1} i.p. daily) the following day. Nor-BNI treatment did not alter any EAE parameters (i.e. disease scores, peak disease) compared to vehicle-treated animals (Figure 1i and Supplementary figure 3e), indicating that treatment with nor-BNI does not affect the progression of EAE. In contrast, blocking KOR with nor-BNI significantly impaired the ability of nalfurafine to enable full recovery consistent with nalfurafine treatment alone (Figure 1i; $P < 0.0001$), although nalfurafine did still provide some therapeutic benefit in terms of reduced disease scores ($P < 0.0001$). Specifically, KOR antagonism fully abolished recovery, with only 12.5% recovery (1/8 $P < 0.01$) compared to
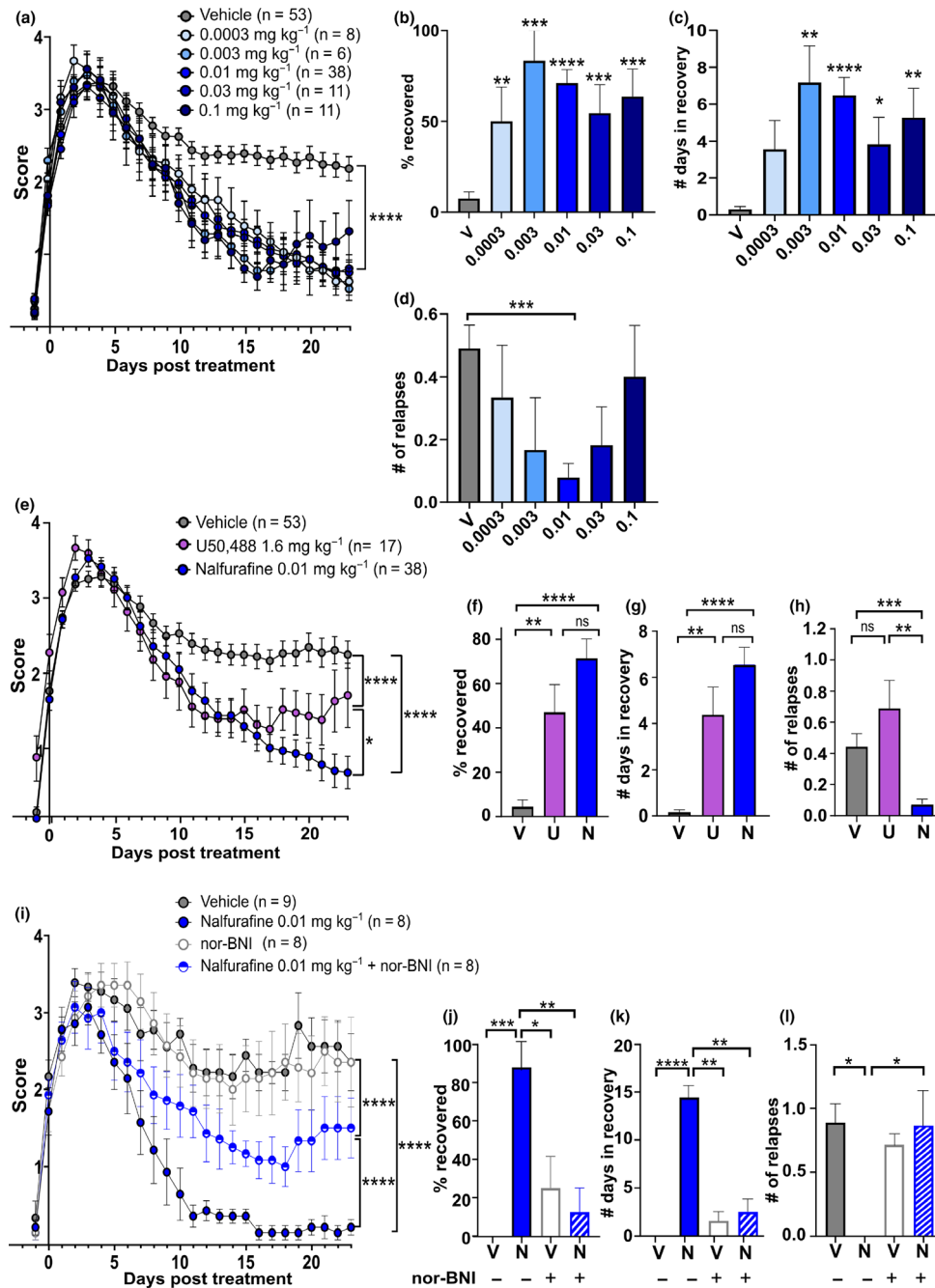
Figure 1. Treatment with nalfurafine was more effective than U50,488 at enabling functional recovery of EAE. Data are mean ± SEM. A 2-way (ANOVA) test was used for scoring data. A 1-way ANOVA with Holm–Sidak's multiple comparison test was used for comparing treatment doses to vehicle. *$P < 0.05$ **$P < 0.01$, **$P < 0.001$, ****$P < 0.0001$. **(a)** Disease scores of nalfurafine (0.0003–0.1 mg kg^{-1}) treated animals from disease onset (score ≥ 1) to 23 dpt. Scores aligned to the day of disease onset (day 0 post-treatment). Mice were treated i.p daily with vehicle, or nalfurafine. Results are combined from 12 independent experiments ($n = 6$–53, as indicated). **(b)** Percentage recovery to 23 dpt (recovery = score ≤ 0.5). **(c)** Number of days in recovery to 23 dpt. **(d)** Number of relapses per mouse to 23 dpt (relapse = increase by 1 full point from the lowest score of remission). **(e)** Disease scores of KOR agonist treated EAE to 23 dpt. Mice were treated i.p. daily with vehicle, U50,488 at 1.6 mg kg^{-1}, or nalfurafine at 0.01 mg kg^{-1}. Scores aligned to day of disease onset. Results are combined from 12 independent experiments ($n = 17$–53). **(f)** Percentage recovery to 23 dpt. **(g)** Number of days in recovery to 23 dpt. **(h)** Number of relapses per mouse to 23 dpt. **(i)** Animals treated i.p. with vehicle or nor-BNI (10 mg kg^{-1}) to induce full KOR antagonism or vehicle, this continued once weekly thereafter. Animals also treated with i.p. injection one day following nor-BNI treatment with vehicle or nalfurafine (0.01 mg kg^{-1}), and daily treatment continued thereafter. Results are combined from 2 independent experiments ($n = 8$ or 9). **(j)** Percentage recovery to 23 dpt. **(k)** Number of days in recovery 23 dpt. **(l)** Number of relapses per mouse 23 dpt.

nalfurafine alone (87.5%; 7/8) (Figure 1j), and days spent in recovery (1.8 ± 1.35; $P < 0.01$) compared to nalfurafine alone (14.4 ± 1.17) (Figure 1k). Furthermore, nor-BNI abolished the effect of nalfurafine on the relapse rate in EAE such that the number of relapses per mouse (0.87 ± 0.29) was similar to vehicle (0.89 ± 0.20) (Figure 1l). Interestingly, nalfurafine/nor-BNI-treated mice recovered from EAE-associated weight loss compared to either nor-BNI alone or vehicle (Supplementary figure 3f; $P < 0.01$). These data confirm that KOR contributes to the disease-modifying activity of nalfurafine.

Nalfurafine reduced lesion size and promoted remyelination in EAE

In order to determine whether the observed nalfurafine-mediated recovery was associated with reduced lesion size and/or increased myelin, spinal cord sections were stained with Black Gold II. Using BlackGold II to determine myelin levels, we found a significant increase in myelinated area in nalfurafine-treated mice during chronic EAE (day 45) compared to peak disease (day 18), and this difference was not observed in the vehicle-treated mice (Figure 2b). Similar levels of demyelination were observed at peak disease in the vehicle and nalfurafine-treated groups, which suggests that nalfurafine promoted significant remyelination by day 45. The percentage lesion area in the white matter was measured, (highlighted by the dotted regions in Figure 2a) and showed consistent lesions in vehicle-treated mice (Figure 2c). Although there was a trend suggestive of a reduction in lesion area with nalfurafine treatment at day 45 compared to day 18, it did not reach significance. The number of lesions per mouse at day 45 compared to peak disease in the nalfurafine-treated groups was also reduced, but did not reach significance (Figure 2d).

For high-resolution analysis of myelin integrity in the chronic phase of EAE, myelin thickness and myelinated axon numbers were assessed by transmission electron microscopy (TEM) with representative images shown in Figure 2e. To explore the impact of nalfurafine treatment on myelination of axons, we compared the percentage of myelinated and unmyelinated axons between treatment groups (Figure 2f). There was an increase in the percentage of myelinated axons (86.4% ± 1.6; $P < 0.05$) and a decrease in the percentage of unmyelinated axons (13.6% ± 1.6;

$P < 0.001$) in the group administered nalfurafine in comparison to vehicle (69.6% ± 0.26 myelinated; 30.4% ± 0.26 unmyelinated). Demyelinated and remyelinating axons in the EAE spinal cord are identified by a thinner myelin sheath (i.e. higher g-ratio), compared to those in a healthy spinal cord, which have a g-ratio somewhere below 0.8. Figure 2g shows a scatter plot of g-ratio as a function of axon diameter for each group, with trend lines reported. Lower g-ratios were seen for all axon diameters in both healthy and nalfurafine-treated mice compared to vehicle. We observed that most healthy axons had a g-ratio in the range of 0.6–0.8, as expected (0.68 ± 0.003). Axons from vehicle-treated EAE mice had an increased mean g-ratio compared to healthy, indicating demyelination (0.75 ± 0.004; $P < 0.0001$) (Figure 2h). The mean g-ratio of axons from nalfurafine-treated animals were significantly lower than vehicle (0.70 ± 0.002; $P < 0.0001$), and closer to healthy g-ratios, indicating increased myelination. To determine the extent of demyelination in these groups, we defined a g-ratio above 0.8 as demyelinated or remyelinating, according to Mei *et al.* (2016), and found that most axons in the healthy group fell below the 0.8 threshold (9.9%; Figure 2i). Vehicle-treated animals had a significantly higher number of axons above 0.8 (22.4%) compared to nalfurafine (11.5%), which was similar to healthy. Consequently, our results indicate that nalfurafine effectively promotes remyelination during EAE.

Nalfurafine administration during chronic EAE remained effective at promoting functional recovery

To determine whether nalfurafine could promote remyelination after chronic demyelination, animals were treated from 10 days post-peak (dpp) EAE disease and were randomly assigned to either treatment group according to the time to reach peak disease. We observed that initiating daily treatment with nalfurafine at 0.01 mg kg^{-1} at this chronic EAE stage still enabled significant recovery in EAE (Figure 3a; $P < 0.0001$; scores aligned to disease peak). In this treatment, 23% (3/13) of treated animals reached full functional recovery by day 23 post-treatment, whereas no animals in the vehicle-treated group fully recovered (0/12) (Figure 3b). As expected, there was no difference in peak disease between groups (Supplementary figure 3g). In addition, delayed treatment with nalfurafine promoted recovery from EAE-
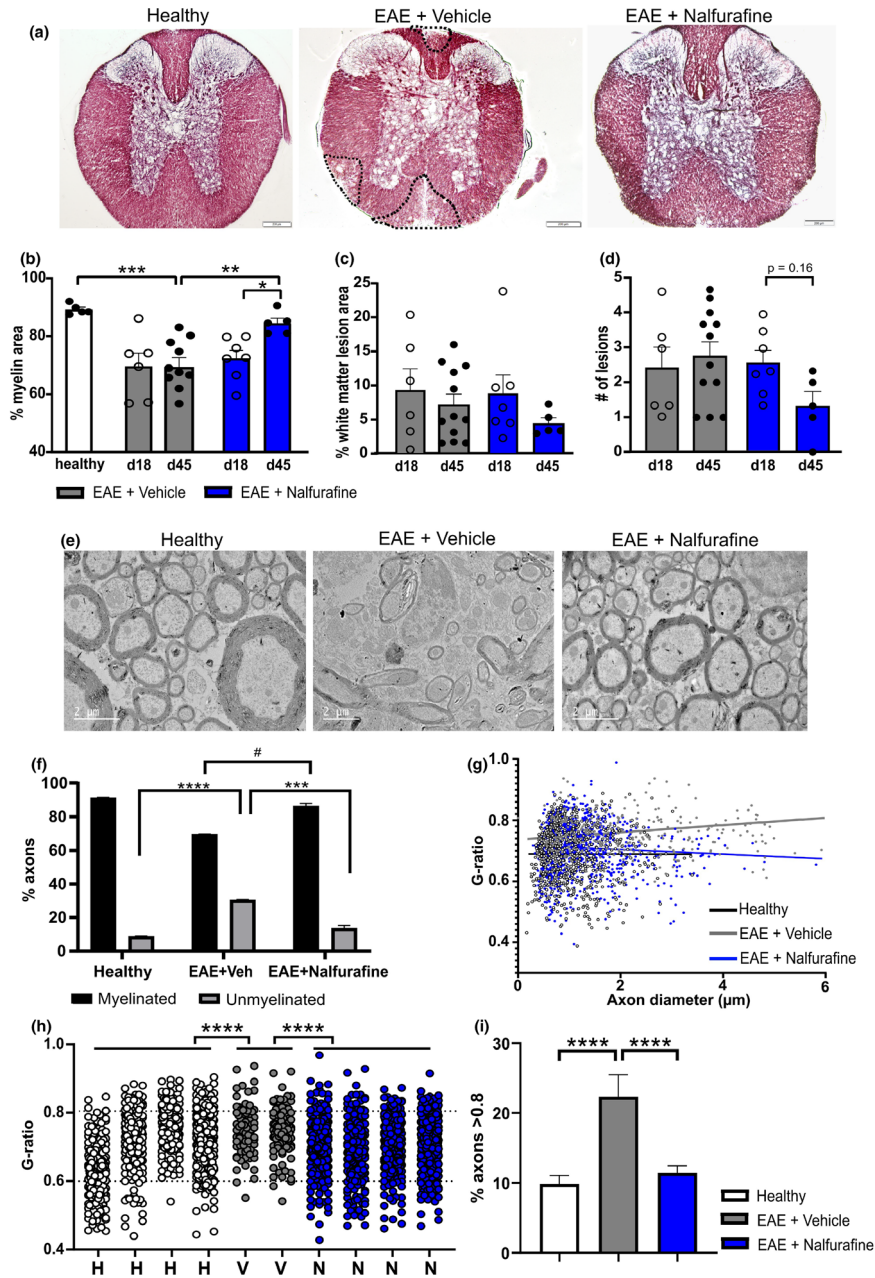
Figure 2. Nalfurafine reduced lesion size and promoted remyelination in EAE. Data are mean ± SEM. A one-way ANOVA with Holm–Sidak's multiple comparison test was used for comparing groups. *$P < 0.05$ **$P < 0.01$, **$P < 0.001$, ****$P < 0.0001$. **(a)** Spinal cord sections assessed by Black Gold II staining. Representative images of spinal cord sections from either age matched healthy animals (-EAE), EAE animals (+EAE) treated with vehicle, or +EAE animals treated with nalfurafine (0.01 mg kg^{-1}) to day 45. Results are shown from 4 independent EAE experiments, $n = 5$–11 mice per group. Each data point represents three sections from descending parts of the cervical spinal cord, averaged per animal. **(b)** Percentage myelin area per animal determined by thresholding. **(c)** Percentage white matter lesion area per animal determined by quantification of total area of lesions in the white matter spinal cord. **(d)** Number of white matter lesions per animal. **(e)** Representative TEM images of spinal cord sections from either; –EAE age matched healthy animals, +EAE treated with vehicle or +EAE nalfurafine (0.01 mg kg^{-1}) to day 45. Scale bar = 2 μm. Results are from 3 independent EAE experiments, $n = 2$–4 mice per group. **(f)** Percentage of myelinated versus unmyelinated axons per group. Myelinated axons #$P < 0.05$ by 1-way ANOVA with Holm–Sidak's multiple comparisons test. Unmyelinated axons ***$P < 0.001$, ****$P < 0.0001$ by 1-way ANOVA with Holm–Sidak's multiple comparisons test. **(g)** Plots of inner axon diameter versus g-ratio (inner axon diameter/outer axon diameter) fit with a linear function. **(h)** G-ratios per animal, along the x-axis each individual animal is defined as H (healthy), V (vehicle) or N (nalfurafine). At least 200 axons per group were analysed. G-ratio analysis on at least 20 images per animal. Significance is determined per treatment group. **(i)** Percentage of total axons with g-ratio of 0.8 or above.

associated weight loss compared to vehicle (Supplementary figure 3h; $P < 0.05$).

To determine whether nalfurafine promoted myelination after chronic demyelination in the EAE model, spinal cord axons were analysed by TEM, and representative images from each treatment group are shown in Figure 3c. We found a decrease in the percentage of unmyelinated axons (14.3% $\pm$ 3.8; $P < 0.01$) in the nalfurafine-treated group in comparison to vehicle (22.9% $\pm$ 5.04) (Figure 3d) as well as an increase in g-ratio in vehicle-treated EAE axons (0.72 $\pm$ 0.004; $P < 0.05$) compared to healthy (0.7 $\pm$ 0.003) (Figure 3e, f). Nalfurafine-treated animals had significantly thicker myelin layers (i.e. lower g-ratios) compared to vehicle-treated mice, and this finding is supported by a decrease in g-ratio (0.69 $\pm$ 0.004; $P < 0.01$) and decreased percentage of unmyelinated axons compared to vehicle (Figure 3f, g). Consistent with previous findings, no difference was detected between nalfurafine-treated and healthy animals in terms of g-ratio or percentage of unmyelinated axons. Taken together, these findings indicate that nalfurafine can promote remyelination even following sustained demyelination in EAE.

CNS-infiltrating immune cells are reduced by daily KOR-agonist administration in EAE

Since nalfurafine displayed significant therapeutic responses in EAE, we assessed whether nalfurafine altered the immune environment contributing to EAE disease reduction. To evaluate immune phenotype, we analysed splenic T-cell and myeloid populations 45 days after EAE induction, (gating strategy in Supplementary figure 4), but found no difference in the proportions of CD4$^+$ T cells, CD8$^+$ T cells, or CD25$^+$ regulatory T cells (Supplementary figure 5a). CD25$^+$CD4$^+$ T cells were confirmed to express FoxP3$^+$, the key Treg transcription factor (Supplementary figure 6). Additionally, there was no difference in the proportion of cells in the myeloid compartment, including CD11b$^+$Ly6G-F4/80^{hi} macrophages, CD11b$^+$Ly6G^{hi} neutrophils, CD11b$^+$Ly6C$^+$ monocytes, or CD11b$^+$CD11c^{hi}I-A/I-E^{hi} dendritic cells (Supplementary figure 5b). Overall, nalfurafine did not alter the major peripheral immune cell populations in the spleen during chronic EAE.

Inflammatory damage in the CNS during MS and EAE is regulated by many cell types including T cells, B cells, neutrophils, monocytes, macrophages, and resident microglia. Figure 4a shows the gating strategy for evaluating immune cell infiltration into the CNS. We found similar infiltration of immune cells (i.e. CD45^{high} cells) at peak disease (day 18) regardless of treatment, but the neuroinflammation was reduced at chronic EAE with nalfurafine treatment compared to vehicle (Figure 4b; $P < 0.05$). This finding indicates that nalfurafine treatment contributes to the resolution of immune cell infiltration in the CNS. To understand if specific immune cell populations were differentially affected, we assessed CD4$^+$ T cells, CD8$^+$ T cells, Tregs, and B cells as a frequency of CD45^{int} microglia using a sequential gating strategy shown in Figure 4c. We also assessed neutrophils, macrophages, monocytes, and dendritic cells as a frequency of CD45^{int}CD11b$^+$ microglia using the sequential gating strategy shown in Figure 4d. The number of CD45^{int}CD11b$^+$ microglia (in myeloid gating strategy) was comparable to CD45^{int} microglia (in lymphocyte gating strategy; Supplementary figure 6). There was no difference in lymphocyte populations between nalfurafine and vehicle-treated groups at peak disease consistent with the similar peak disease scores at day 18 (Figure 4e). During chronic disease, nalfurafine treatment resulted in a significant reduction in both CD4$^+$ and CD8$^+$ T cells ($P < 0.05$), but did not appear to alter either CD25$^+$ Treg or B-cell infiltration into the CNS at chronic EAE. Furthermore, there was no difference in myeloid cell infiltration between nalfurafine and vehicle-treated groups at peak disease or in the recovery phase of EAE (Figure 4f). Overall, nalfurafine treatment alters the CNS immune environment by reducing the infiltration of CD4$^+$ and CD8$^+$ T cells into the CNS, and this reduced T-cell infiltration may contribute to the therapeutic effects of nalfurafine in EAE.

Presence of KOR agonists alters the peripheral T-cell response

Although the abundance of splenic T-cell populations was unaltered by nalfurafine treatment, it was possible that KOR-agonist treatment altered antigen-specific T-cell responses given the reported immunomodulatory properties of KOR agonists.[20] Splenocytes from nalfurafine, U50,488, vehicle-treated EAE animals and healthy controls were isolated at day 45 post-immunisation and stimulated *ex vivo* with either myelin oligodendrocyte glycoprotein (MOG$_{35-55}$) peptide to assess antigen-specific responses or the
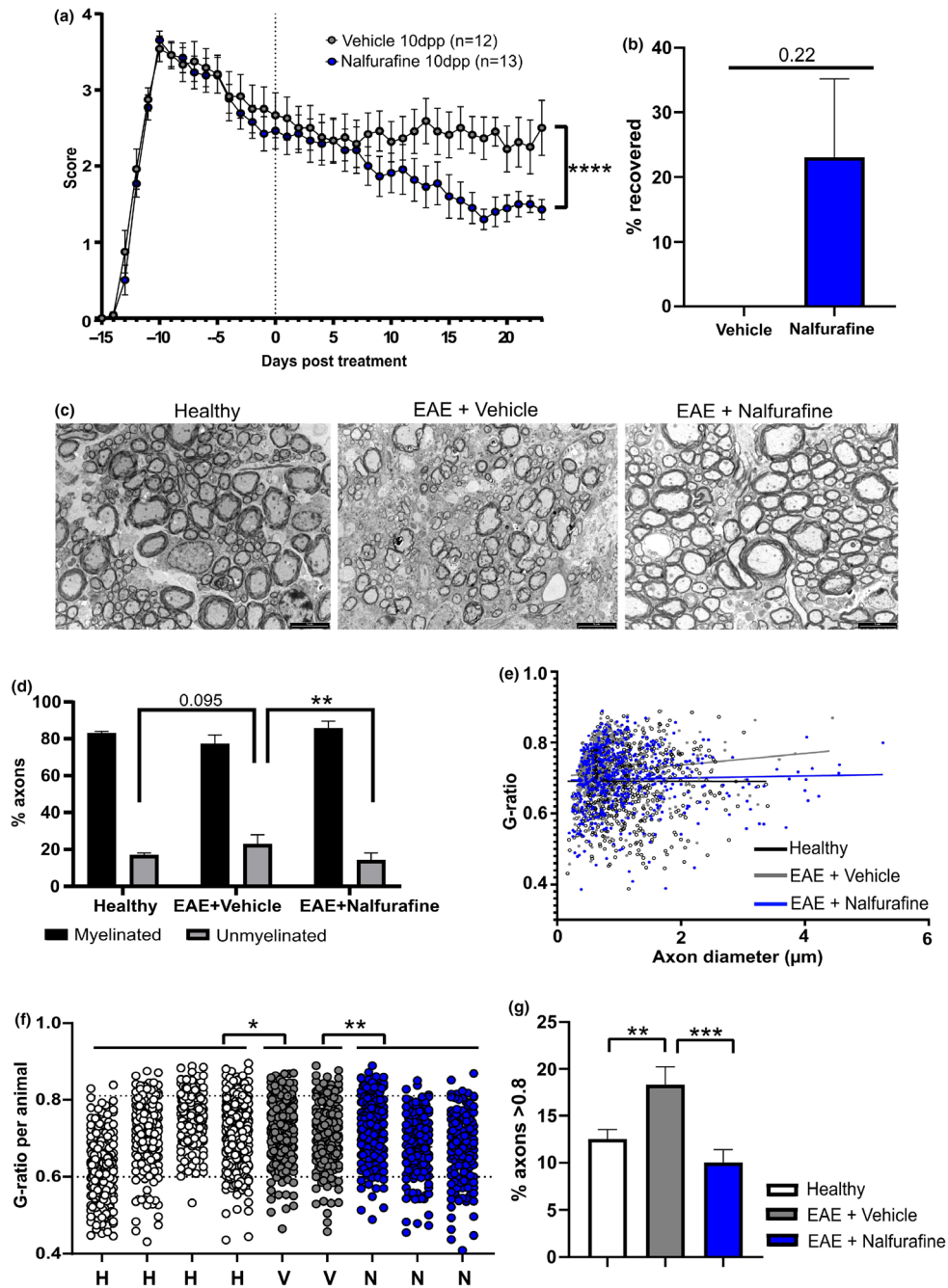
Figure 3. Nalfurafine remained effective in promoting functional recovery in chronic EAE. Data are mean ± SEM. A 2-way (ANOVA) test was used for scoring data. 1-way ANOVA with Holm–Sidak's multiple comparison test for comparing groups. *$P < 0.05$, **$P < 0.01$, **$P < 0.001$, ****$P < 0.0001$. **(a)** Disease scores of nalfurafine-treated EAE from 10 dpp to 23dpt, where scores are aligned to disease peak. Female, C57BL/6 mice were immunised to induce EAE as described and scored daily. Mice were treated from 10 dpp (day 0 post-treatment; indicated by the dotted line at X = 0) with i.p injection daily with vehicle or nalfurafine (0.01 mg kg^{-1}). Results shown are combined from 3 independent experiments (n = 12 or 13). **(b)** Percentage recovery to 23 dpt compared to vehicle (recovery = score ≤ 0.5). **(c)** Representative images of spinal cord sections from either; −EAE age matched healthy animals, +EAE treated with vehicle or +EAE nalfurafine (0.01 mg kg^{-1}). Scale bar = 5 μm. Results shown are from 3 independent EAE experiments, n = 2–4 mice per group. **(d)** Percentage of myelinated versus unmyelinated axons per group. Unmyelinated axons **$P < 0.01$ by 1-way ANOVA with Holm–Sidak's multiple comparisons test. **(e)** Plots of inner axon diameter versus g-ratio (inner axon diameter/outer axon diameter) fit with a linear function. **(f)** G-ratios per animal, along the x-axis each individual animal is defined as H (healthy), V (vehicle) or N (nalfurafine). At least 200 axons per group were analysed. Significance is determined per treatment group. **(g)** Percentage of total axons which have a g-ratio of 0.8 or above.

polyclonal T-cell mitogen, concanavalin A (ConA), which leads to activation of T cells and the production of cytokines. Splenocytes were analysed for intracellular cytokine responses (gating strategy in Supplementary figure 7). Following *in vivo* treatment with KOR agonists and *in vitro* stimulation, no significant changes to CD4$^+$ or CD8$^+$ T-cell frequencies in response to KOR-agonist treatment were found (Supplementary figure 8a, b). In response to ConA stimulation, the percentage of interferon (IFN)γ^+ CD4$^+$ and CD8$^+$ T cells was reduced by daily *in vivo* nalfurafine treatment but not U50,488, suggestive of a dampening of the Th1 response (Figure 5a, b; $P < 0.05$). To determine whether nalfurafine exerted a direct effect on T cells, splenocytes from EAE animals (at day 28) were stimulated with MOG$_{35-55}$ peptide or ConA in the presence of nalfurafine (50 nM), U50,488 (1 μM), or vehicle. These doses were selected to be within a range previously confirmed to have comparative pERK signalling activity[16] and within a range of 10–100 nM found to alter cytokine activity on naïve splenocytes (Supplementary figure 9).[11,16,21] Following *in vitro* KOR agonist treatment, the proportion of CD4$^+$ or CD8$^+$ T-cell populations were similar between groups (Supplementary figure 8c, d), whereas ConA-stimulation in the presence of nalfurafine significantly decreased the percentage of IFNγ^+ CD4$^+$ T cells compared to vehicle (Figure 5c). Furthermore, both nalfurafine and U50,488 significantly reduced IFNγ^+ CD8$^+$ T cells following MOG$_{35-55}$ stimulation and ConA stimulation (Figure 5d).

In contrast to IFNγ, nalfurafine treatment *in vivo* or *in vitro* significantly reduced MOG$_{35-55}$-specific interleukin (IL)-17A expression by CD4$^+$ T cells (Figure 5e, f; $P < 0.01$), and while U50,488 treatment appeared to reduce IL-17A production, the effect did not reach significance. We also observed no difference in IL-17A expression in CD8$^+$ T cells (Supplementary figure 8e, f). Finally, no change in IL-10 expression in CD4$^+$ and CD8$^+$ T cells of EAE animals treated *in vivo* was detected (Supplementary figure 8g, h); however, IL-10 increased following nalfurafine treatment *in vitro* compared to U50,488 in unstimulated CD4$^+$ and CD8$^+$ T cells (Figure 5g, h; $P < 0.05$). These data, taken together, support immunomodulation by KOR agonists with nalfurafine having a more significant effect than U50,488 in shifting the immune environment away from Th1 and Th17 to a more regulatory response.

Nalfurafine drives remyelination in the cuprizone model of disease

Since nalfurafine promoted functional recovery and reduced CNS-infiltrating immune cells in EAE, we assessed the effects of nalfurafine in the non-immune-mediated demyelination model, the cuprizone (CPZ) model. In this model, shown in Figure 6a, mice were fed a CPZ diet for 42 days to induce demyelination in the brain. The animals were treated with nalfurafine or vehicle 7 days before returning to standard pelleted chow until the experimental endpoint (day 70). Representative TEM images of the corpus callosum collected at the experimental endpoint are shown in Figure 6b, with 2 animals per group assessed. There was a significant increase in the percentage of myelinated axons in the healthy corpus callosum (80.7% ± 2.0) compared to vehicle (71.2% ± 2.2; $P < 0.05$), while treatment with nalfurafine significantly increased myelinated axons (80.4 ± 1.2; $P < 0.05$) compared to vehicle. Moreover, the percentage of myelinated axons in the nalfurafine-treated corpus callosum was similar to healthy. There was also a significant decrease in the percentage of unmyelinated axons (19.5% ± 1.0) in the group administered nalfurafine in comparison to the CPZ vehicle-treated group (28.8% ± 2.2; $P < 0.001$), while the percentage of unmyelinated axons in the nalfurafine-treated corpus callosum was again similar to healthy (19.6 ± 2.2) (Figure 6c). The g-ratio of the animals administered nalfurafine (0.73 ± 0.076) significantly decreased in comparison to the CPZ control group (0.76 ± 0.0057; $P < 0.01$) (Figure 6d, e). These results indicate that nalfurafine treatment significantly enhanced remyelination in the corpus callosum following demyelination, even in the absence of immune cells.

DISCUSSION

Recent work has shown that KOR agonists significantly alleviate the symptoms of EAE and promote repair of damaged myelin,[11] but clinical translation of the findings has been hampered by the poor side-effect profile of these KOR agonists. This study aimed to evaluate whether a clinically-approved KOR agonist, nalfurafine, would be an appropriate candidate to promote repair and remyelination during MS. This study demonstrated that nalfurafine, a potent KOR agonist, improves
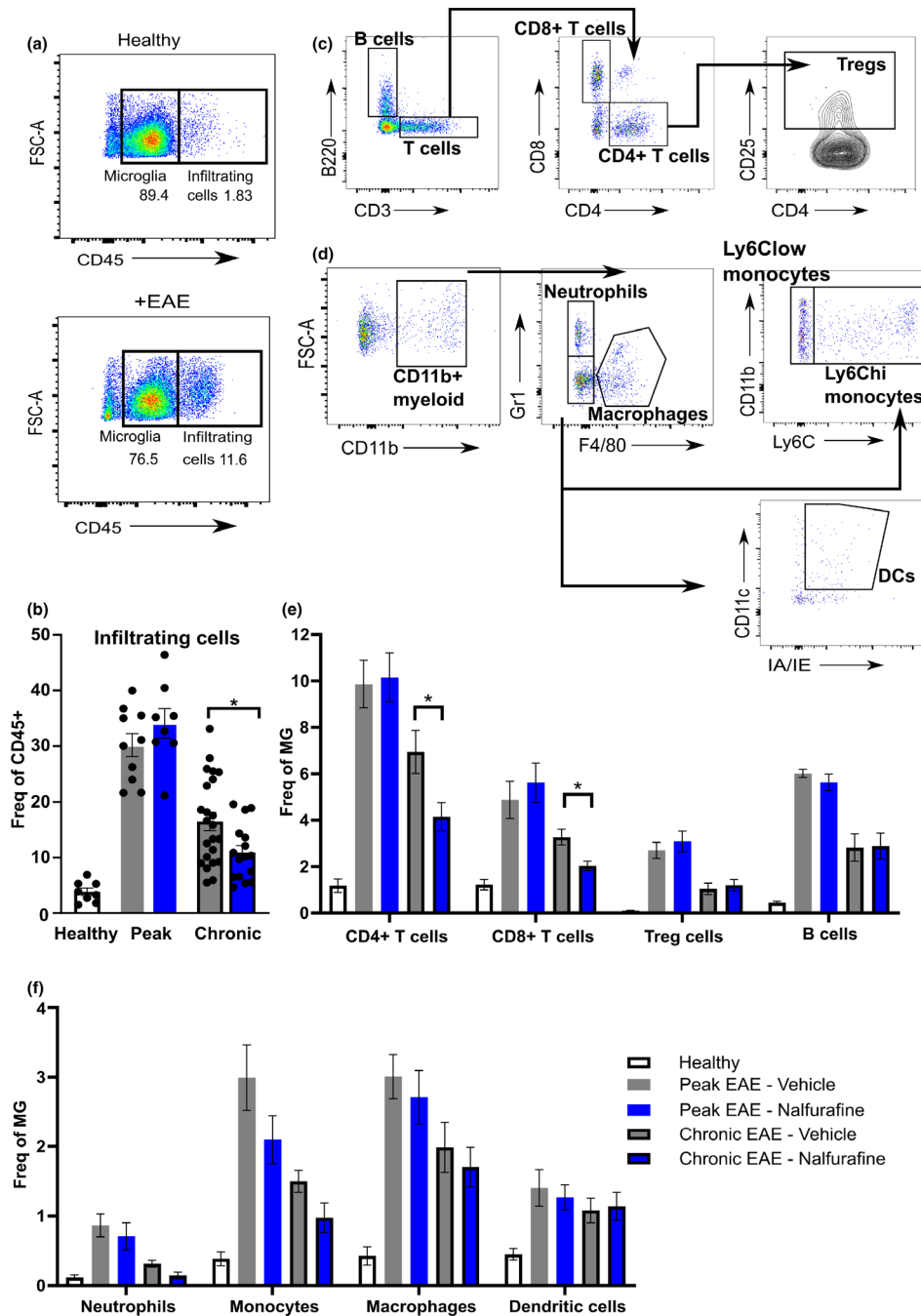
Figure 4. CNS-infiltrating immune cells were reduced by daily KOR-agonist administration in EAE. Shown are the results from 7 independent experiments with 8–23 mice per group. Data are mean ± SEM. The non-parametric Mann–Whitney test was used for comparing either peak EAE or chronic EAE groups. *$P < 0.05$. **(a)** Analysis of lymphocyte populations from healthy, vehicle and nalfurafine (0.01 mg kg^{-1}) treated brain tissue. All infiltrating immune cells were identified by CD45^{high} expression. The relative number of cells is expressed as a ratio to microglia (CD45^{int}CD11b$^+$). **(b)** Infiltrating cells identified by CD45^{high} expression, at either day 18 (peak disease) or day 45 (recovery) post-immunisation. **(c)** Identification of CNS-infiltrating lymphocyte immune cell types by a sequential gating strategy. Identification of B cells (CD45^{high}CD3-B220$^+$), CD4$^+$ T cells (CD45^{high}B220$^-$CD3$^+$CD4$^+$), CD8$^+$ T cells (CD45^{high}B220$^-$CD3$^+$CD8$^+$), and Tregs (CD45^{high}B220$^-$CD3$^+$CD4$^+$CD25$^+$). **(d)** Identification of CNS-infiltrating myeloid immune cell types by a sequential gating strategy. Identification of myeloid cells (CD45^{high}CD11b$^+$), neutrophils (CD45^{high}CD11b$^+$GR1$^+$), macrophages (CD45^{high}CD11b$^+$F4/80$^+$), DCs (CD45^{high}CD11b$^+$Gr1-F4/80-CD11c$^+$IA/IE$^+$) and monocytes (CD45^{high}CD11b$^+$Gr1-F4/80$^-$CD11c$^+$IA/IE + Ly6C$^{high/low}$). **(e, f)** Analysis of immune populations in the brain. The relative number of cells is determined as a ratio to microglia (CD45^{int}CD11b).

clinical recovery when administered at the onset of symptoms as well as in the chronic phase of EAE. Moreover, the potential of nalfurafine as a therapeutic option is highlighted by its immunomodulatory effects as well as its neuroprotective effects, which occur independently. Finally, we report that the disease-modifying effects of nalfurafine occur over a wide range of doses and are superior to the prototypic KOR agonist, U50,488.

While nalfurafine provides a significant benefit over a wide range of doses (0.1–0.0003 mg kg^{-1}), the 0.01 mg kg^{-1} dose appears to be the most effective at promoting disease recovery, enhancing the time to recovery, and reducing relapse rate. While U50,488 promoted recovery in EAE as reported previously,[11] this study is the first to show that therapeutic administration of U50,488 reduced EAE. Interestingly, while both nalfurafine and U50,488 reduced disease and enhance recovery, we also observed that in contrast to nalfurafine, U50,488 enhanced the relapse rate. The limited effect on disease relapse suggests that the immunomodulatory effects of U50,488 may not fully regulate the on-going neuroinflammatory response.

To verify that nalfurafine alleviates the symptoms of EAE through KOR activation, we blocked the KOR with a highly selective and potent KOR antagonist, nor-BNI, a dimeric naltrexone derivative used as a standard tool in opioid pharmacology.[22,23] We showed that the effect of nalfurafine was significantly inhibited, reflected by disease scores, as well as in recovery and relapse rates. Previous research has revealed that the antinociceptive effects of the KOR agonist U50,488 and the salvinorin A analog, Mesyl Sal B can be blocked by a single injection of nor-BNI (10 mg kg^{-1} i.p.) in rats and mice.[24,25] Interestingly, the effect of nalfurafine was not completely abolished to the levels of the vehicle-treated animals in terms of disease scores, with the nalfurafine plus nor-BNI animals performing significantly better than the vehicle or nor-BNI single treatment. Although one possible explanation could be that these weekly injections of nor-BNI only partially blocked the KOR, previous studies have demonstrated that weekly injections of nor-BNI are sufficient to completely block KOR activity due to the long-lasting and selective effect of nor-BNI (i.e. a half-life of ~14 days in mice).[26,27] Alternatively, these data could indicate that there is another additional mechanism, by which nalfurafine reduces EAE disease, which is independent of nor-BNI inhibition.

In MS, remyelination is impaired during the chronic stage as a result of OPC differentiation into mature OLs being halted.[28,29] Promoting OPC maturation into myelinating OLs is therefore crucial for myelin repair. Previous reports[11,21] demonstrated that a variety of KOR agonists could improve oligodendrocyte differentiation and myelination in EAE. These reports are consistent with our study which showed that nalfurafine-treated animals had a greater myelinated area upon disease recovery (45 d.p.i) in the spinal cord compared to vehicle-treated animals (45 d.p.i). It is important to note that extensive demyelination is evident at peak disease (18 d.p.i), and is equal between treatment groups, suggesting that nalfurafine does not inhibit immune-mediated demyelination in the first few days of administration. A large sample size of 5–10 animals per treatment group give a robust indication that nalfurafine is driving remyelination in EAE. However, within these analyses, there was a limit of 3 sections of the spinal cord per mouse averaged for the assessment. Future analysis with a larger sampling region of the spinal cord would ensure that lesions are not missed, and give a conclusive representation of the full extent lesion areas in each animal.

By TEM analysis, we observed that spontaneous remyelination is ineffective in EAE to day 45, represented by an increase in the percentage of unmyelinated axons compared to myelinated axons in the vehicle-treated group, in addition to the high percentage of demyelinated axons having a g-ratio above 0.8. In contrast, nalfurafine-treated EAE animals had a recovery in the number of myelinated and a decrease in unmyelinated axons, suggesting nalfurafine can restore myelination and axon integrity to healthy levels. This finding is supported by the reduction in the g-ratio by nalfurafine compared to vehicle treatment, which indicates remyelination. As g-ratios have been presented for each individual animal in the analyses, there appears to be variations in g-ratio in the healthy samples. Larger axons tend to have higher g-ratios. This is the case in this analysis, where g-ratio variability is evident depending on mean axon diameter (Supplementary figure 10). Previous literature has reported that axonal diameters are generally
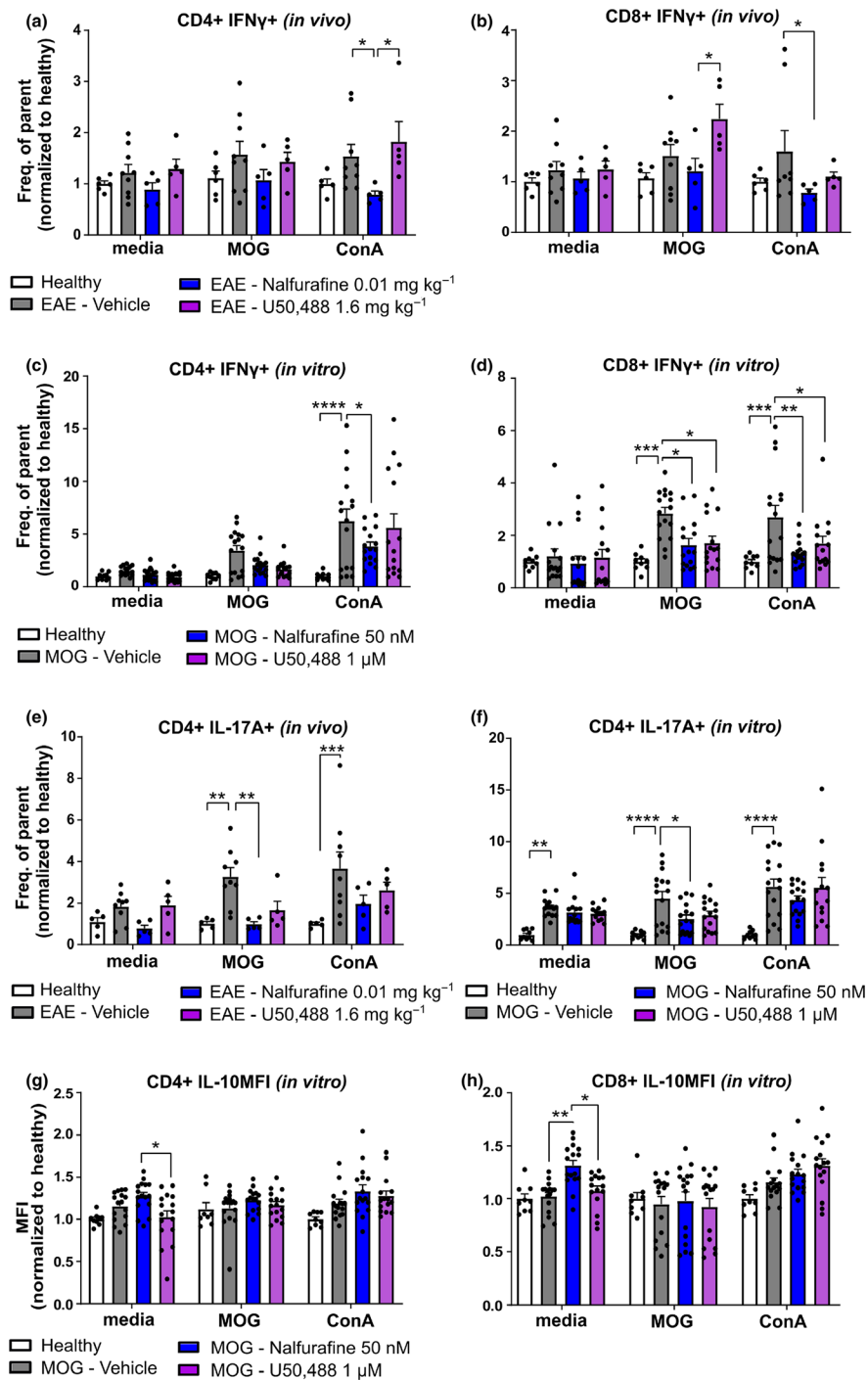
Figure 5. Presence of KOR agonists alters the peripheral T-cell response. Data are mean ± SEM. The 1-way ANOVA with Holm–Sidak's multiple comparison test was used for comparing treatments within each stimulation. *$P < 0.05$, **$P < 0.01$, **$P < 0.001$, ****$P < 0.0001$. **(a, b)** CD4^{+} and CD8^{+} T-cell intracellular interferon (IFN)γ from splenocytes of EAE animals treated daily from onset with vehicle, nalfurafine (0.01 mg kg^{-1}) or U50,488 (1.6 mg kg^{-1}). **(c, d)** CD4^{+} and CD8^{+} T-cell intracellular IFNγ from splenocytes of MOG$_{35-55}$ immunised animals to day 28. Splenocytes were treated *in vitro* with vehicle (0.01% DMSO), nalfurafine (50 nM) or U50,488 (1 μM) for 72 h alongside stimulations. **(e)** CD4^{+} T-cell intracellular interleukin (IL)-17A (as frequency of parent, CD4^{+}) from splenocytes of EAE animals treated daily from onset with KOR agonists. **(f)** CD4^{+} T-cell intracellular IL-17A (as frequency of parent, CD4^{+}) from splenocytes of MOG$_{35-55}$ immunised animals to day 28 and treated *in vitro* with KOR agonists. **(g, h)** CD4^{+} and CD8^{+} T-cell intracellular IL-10 as mean fluorescence intensity (MFI) from splenocytes of MOG$_{35-55}$ immunised animals to day 28 and treated *in vitro* with KOR agonists.

< 2 μm, with a mean g-ratio of 0.6–0.7.[11,21] Taking this into account, g-ratios for healthy animals fell within the range of typical g-ratios.

In MS, chronic and continuous inflammation and demyelination drive the long-term progression of deficits, and this process is modelled by EAE.[30] We found that nalfurafine was effective in this chronic phase of EAE, indicating that it not only halts further myelin damage but also promotes myelin recovery after chronic demyelination. While there was no significant difference in the number of myelinated axons between the EAE and healthy animals, spontaneous remyelination may be occurring during chronic EAE, allowing for remyelination of demyelinated axons. However, there is a clear increase in the number of unmyelinated axons in vehicle-treated EAE compared to the nalfurafine-treated group, which correlates to the increase in g-ratio. Taken together, these data suggest that nalfurafine may be a promising candidate for the treatment of chronic demyelinating disease such as MS, where there is continuous inflammation and the accumulation of neurological deficits.

Our results indicate that nalfurafine treatment had little effect on the major peripheral immune populations, which is consistent with previous reports using U50,488 during EAE.[11] As EAE induces neuroinflammation, we explored the effects of nalfurafine treatment on CNS-infiltrating immune cells. By comparing CNS infiltrates at peak EAE and chronic disease, we showed that EAE-associated infiltration is significantly reduced by daily nalfurafine treatment. These findings are consistent with Tangherlini *et al*.,[31] who observed a reduction in CD45$^+$ cells in EAE following KOR agonist treatment, which was absent in KOR-deficient mice. In both MS and EAE, effector T cells cross the BBB into the CNS to promote inflammation leading to demyelination and axonal damage. We found that nalfurafine treatment led to a significant reduction of infiltrating CD4$^+$ T cells and CD8$^+$ T cells, which are considered major pathogenic contributors to EAE.[30,32] Importantly, this study is the first to report on the effects of KOR agonists on CNS infiltrate subsets when administered after the onset of disease and supports the potential of nalfurafine to decrease T cell-mediated neuroinflammation within the CNS.

The immunomodulatory properties of KOR agonists have previously been explored,[20,31,33] and

this work provides evidence to suggest that the opioid system can interact with the immune system.[34] For example, Tangherlini *et al*.[31] demonstrated that KOR agonist treatment regulates effector T-cell activation following EAE and the effect is dependent on binding to KOR. Our study revealed MOG$_{35–55}$-specific downregulation of Th17 responses by nalfurafine but not U50,488. Previous studies did not find that U50,488 altered immune responses such as the percentage of pathogenic cells in the CNS or CD4$^+$ T-cell subsets or cytokine secretion.[11] We also found that MOG$_{35–55}$-specific Th1 responses were not significantly affected by nalfurafine, although ConA-induced IFNγ expression was significantly reduced following *in vivo* or *in vitro* exposure. Our findings along with those of Du *et al*. suggest that U50,488 has only modest immunomodulatory activity, and highlight that different KOR agonists may have distinct patterns of activity.[11] Further work is necessary to investigate the mechanisms of action of nalfurafine on the CNS.

IFNγ is typically known to promote differentiation of Th1 cells, directly contributing to neuroinflammation in MS.[35] Additionally, IFNγ production by CD8$^+$ T cells has been reported as an important factor driving EAE and MS,[36,37] with one particular study showing a significant excess of IFNγ-producing CD8$^+$ T cells in MS lesions.[38] We saw significantly reduced expression of polyclonally-induced IFNγ in both CD4$^+$ and CD8$^+$ T cells exposed to nalfurafine *in vivo* or *in vitro*. Additionally, IL-17A, another potent effector in the pathogenesis of EAE,[39,40] was significantly reduced in a MOG$_{35–55}$-specific manner by *in vitro* and *in vivo* exposure to nalfurafine. Finally, IL-10, which is recognised to suppress the development of EAE,[41,42] was increased in CD8$^+$ T cells following *in vitro* nalfurafine treatment. These CD8$^+$ T cells may exhibit a regulatory function with cytokines like IL-10 promoting immune response resolution.[43] These data highlight the influence of KOR agonists like nalfurafine on T-cell effector functions after *in vitro* and *in vivo* exposure.

Non-immune demyelination occurs in the progressive form of MS and the CPZ-mediated demyelination model is believed to recapitulate this pathology. This animal model induces oligodendrocyte apoptosis and demyelination that is reproducible in a highly temporal and spatial manner within the corpus callosum. Although our results show no significant difference in g-ratio
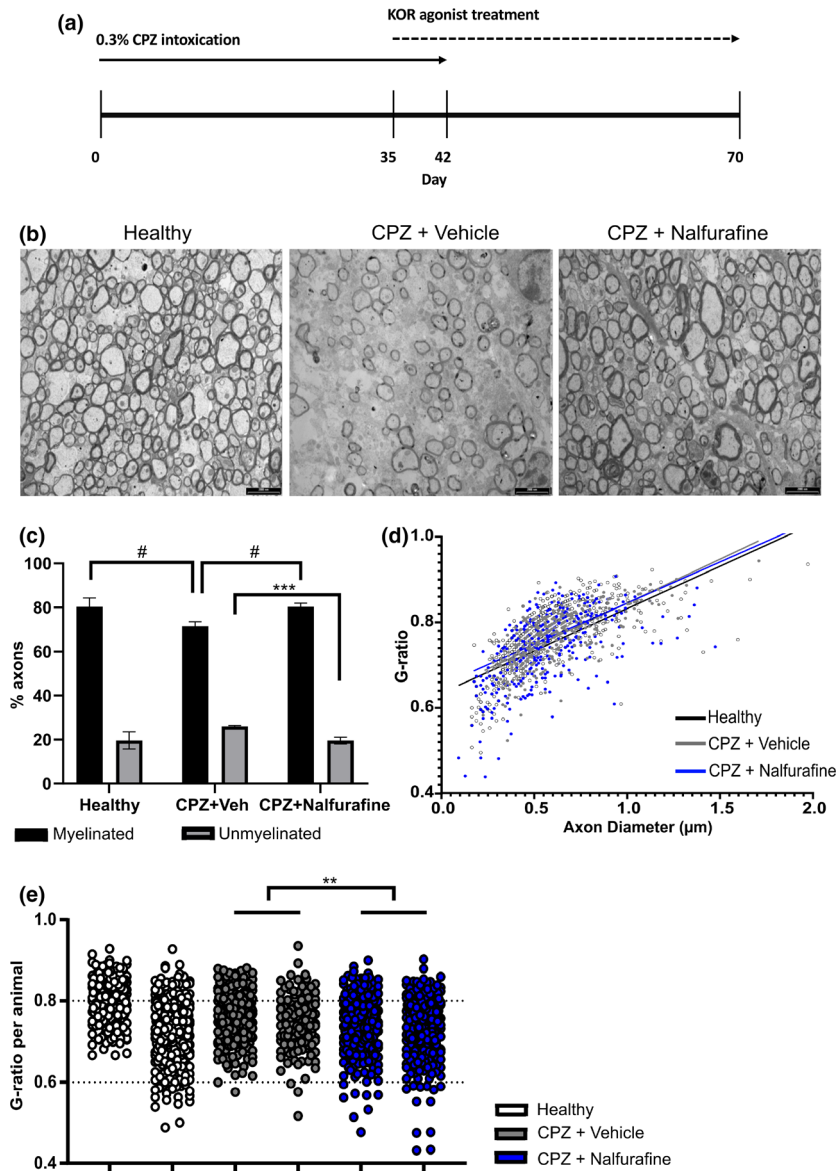
Figure 6. Nalfurafine drives remyelination in the cuprizone model of disease. Data are mean ± SEM. The 1-way ANOVA with Holm–Sidak's multiple comparison test was used for comparing groups. *$P < 0.05$, **$P < 0.01$, **$P < 0.001$, ****$P < 0.0001$. **(a)** CPZ treatment timeline. Mice were fed a cuprizone diet for 42 days to induce demyelination in the brain. The animals were treated with nalfurafine or vehicle 7 days before the mice returned to standard pelleted chow for the duration of 35 days. **(b)** Representative electron micrographs of myelin rich areas within the midline sector of the corpus callosum. Electron micrographs were taken at 5,800 x magnification; 5 images per animal from $n = 2$ mice per group were analysed for g-ratio and % myelinated vs unmyelinated axons. At least 200 axons per group were analysed, from at least 20 images per animal. Scale bar = 2000 nm. **(c)** Percentage of myelinated and unmyelinated axons of all treatment groups. Myelinated axons #$P < 0.05$ by 1-way ANOVA with Holm–Sidak's multiple comparisons test. Unmyelinated axons ***$P < 0.001$ by 1-way ANOVA with Holm–Sidak's multiple comparisons test. **(d)** Plots of inner axon diameter versus g-ratio (inner axon diameter/outer axon diameter) fit with a linear function. **(e)** G-ratios per animal, along the x-axis each individual animal is defined as H (healthy), V (vehicle) or N (nalfurafine). At least 200 axons per group were analysed, from at least 5 images per animal. Significance is determined per treatment group.

between the CPZ and healthy corpus callosum, there was a significant decrease in the percentage of myelinated axons in the CPZ corpus callosum. A clear relationship between axonal diameter and

g-ratio has been reported where larger fibres tend to have higher g-ratios and, therefore, thinner myelin sheaths. One of the animals in the healthy group had an average axonal diameter and g-ratio

of 0.714 μm and 0.80, respectively (Supplementary figure 10). Previous literature has reported that the average axonal diameter and g-ratio in the midline section of the murine corpus callosum is 0.6 μm and 0.75, respectively.[44,45] This suggests that larger fibres were analysed in the corpus callosum of this healthy animal, which could contribute to the high g-ratio observed. The corpus callosum from nalfurafine-treated mice showed a significant decrease in g-ratio in comparison to vehicle-treated CPZ and healthy mice, suggesting an increase in myelin thickness. We also observed an increase in the percentage of myelinated axons and a decrease in the percentage of unmyelinated axons, which reflects what we observed in nalfurafine-treated EAE mice. These data demonstrate that nalfurafine is capable of promoting remyelination following non-immune, as well as immune-mediated demyelination.

Overall, our results indicate that nalfurafine is effective over a wide range of doses when administered therapeutically in EAE with the 0.01 mg kg^{-1} dose providing the greatest and most sustained rate of recovery, with few relapses in a KOR-dependent manner. Nalfurafine is also more effective compared to U50,488 and maintains therapeutic potential even after chronic demyelination in EAE. Nalfurafine has a beneficial effect on neuroinflammation by CD4$^+$ and CD8$^+$ T cells, which may contribute to functional recovery seen in EAE, and this reduction in immune cell infiltration may be enabled by the reduction in Th1 and Th17 response and shift towards a more regulatory environment. Finally, this work highlights the promise of nalfurafine as a treatment with both neuroprotective and immunomodulatory potential for MS as demonstrated by enhanced repair in both immune- and non-immune-mediated models of demyelination.

METHODS

Animals

Female C57BL/6J mice (Jackson laboratory; RRID: IMSR_JAX:000664) were purchased from the Biomedical Research Unit of the Malaghan Institute of Medical Research (Wellington, NZ) or bred in-house and housed in the Victoria University of Wellington PC2 animal facility at a 14 h dark–10 h light cycle. Food and water were available *ad libitum*. Animals were used 8–12 weeks of age for EAE and 8 to 14 weeks for the cuprizone model.

Ethics statement

All of the experiments with animals were carried out in the School of Biological Sciences Animal Facility at Victoria University of Wellington and were approved by the Victoria University of Wellington Animal Ethics Committee (2014-R23 & 25295) for EAE and (24383) for cuprizone.

Drugs

Nalfurafine and U50,488 were synthesised using previously published procedures. Norbinaltorphimine (nor-BNI) (≥ 98% purity by HPLC) was purchased from Tocris Bioscience (Bristol, UK).

EAE induction and treatments

Mice were immunised subcutaneously (s.c.) in the rear flanks with myelin oligodendrocyte glycoprotein (MOG)$_{35–55}$ peptide (50 μg per mouse; Genescript, Piscataway, NJ USA) in complete Freund's adjuvant (Sigma, St. Louis, MO USA) containing 500 μg per mouse heat-inactivated *Mycobacterium tuberculosis* H37Ra (Fort Richard, Auckland, NZ) and injected intraperitoneally (i.p.) with pertussis toxin (200 ng per mouse; List Biochemicals, Campbell, CA USA) on days 0 and 2. In all EAE experiments, mice were weighed and scored daily by an examiner who was blinded to the treatment assignment. EAE scoring is as follows: 0, normal; 1, partial tail paralysis; 2, full tail paralysis; 3, paralysis in one hind limb; 4, paralysis in both hind limbs; and 5, moribund. Mice which reached a sustained score of 4.5 (paralysis in both hind limbs; weakness in front limbs) or above were removed from the experiment. Treatments were blinded throughout the experiment and initiated at disease onset (score ≥ 1) or 10 days after peak disease. Mice were allocated consecutively to each treatment group upon disease onset to ensure the treatment regime remained even across groups. Drugs and the vehicle control were administered daily i.p. in saline: DMSO:Tween80 in a ratio of 8:1:1. Animals were treated daily either from disease onset or 10 days post-peak with either nalfurafine (0.1–0.0003 mg kg^{-1} i.p.) or U50,488 (1.6 mg kg^{-1} i.p). Treatment with the selective KOR antagonist nor-BNI was performed weekly at 10 mg kg^{-1} i.p. with the first dose on the day of disease onset, followed by daily KOR treatments from 24 h post-nor-BNI treatment. EAE experiments following nalfurafine and U50,488 treatment are collated from a total of 17 independent experiments (*n* = 2–7 animals per treatment per experiment). EAE experiments following nor-BNI and nalfurafine treatment are collated from 2 independent experiments (*n* = 4 or 5 animals per treatment per experiment). EAE experiments following delayed nalfurafine treatment are collated from 3 independent experiments (*n* = 2–7 animals per treatment per experiment).

CPZ-induced demyelination

Pelleted chow was ground to a powder using a food processor and mixed with 0.3% cuprizone (CPZ) (Sigma-Aldrich). Approximately 25 g of the mixture was placed in the cages and replaced daily for 42 days. The naïve group

received powdered food with no CPZ. After 42 days of CPZ intoxication, the animals were returned to standard pelleted chow.

Between day 35 and 69, drugs were administered vehicle or nalfurafine (0.01 mg kg^{-1} i.p.) at 5 μL g^{-1} of body weight daily using a 29-gauge needle. All drugs were dissolved in a saline:DMSO:Tween80 in a ratio of 8:1:1. The healthy mice were administered daily vehicle treatment (i.e. saline:DMSO:Tween80).

Primary cell isolation into single-cell suspension

Following CO_2 euthanasia, brains and spleens were isolated and processed into a single-cell suspension for flow cytometry. Brain was mashed through a 70-μm cell strainer and centrifuged at 760 x *g* for 5 min. Brain cell pellets were resuspended in 37% Percoll^{TM} (Sigma-Aldrich) gradient and centrifuged at 760 x *g* for 30 min without brakes. The myelin layer was removed, the supernatant removed, and the pellet resuspended for cell counting.

Spleen was mashed through a 70-μm cell strainer and centrifuged at 760 x *g* for 5 min, the pellet was loosened and red blood cells removed using Red Cell Lysis buffer (Sigma-Aldrich) for 2 min. The number of viable cells was counted using the trypan blue exclusion assay. Cells were cultured at 10^6 cells mL^{-1} in complete T-cell medium (Dulbecco's minimal essential medium, 10% FCS, 100 U mL^{-1} penicillin plus 100 μg mL^{-1} streptomycin, 10 nM HEPES, 2 mM L-glutamine, and 50 μM 2-mercaptoethanol; all from Invitrogen, Carlsbad, CA).

Analysis of cytokines

Splenocytes were plated in complete T-cell medium in a flat-bottomed 96-well plate (Corning, NY USA) and stimulated with medium, MOG$_{35-55}$ peptide (27 μg mL^{-1}) or Concanavalin A (ConA) (1 mL^{-1}; Sigma-Aldrich). Nalfurafine (50 nM), U50,488 (1 μM), or vehicle (0.01% DMSO) was added before incubation for 72 h at 37 °C and 5% CO_2. For intracellular cytokine analysis, splenocyte cultures were stimulated with phorbol 12-myristate 13- acetate (PMA; 50 ng mL^{-1}; Sigma-Aldrich) and ionomycin (500 ng mL^{-1}; Sigma-Aldrich) in the presence of GolgiStop/Monensin (1 μg/10^6 cells; BD Biosciences, NJ) for 4 h at 37 °C and 5% CO_2 before preparing for flow cytometry.

Flow cytometry

Cells were incubated with Fc Block (1 μg/10^6 cells; 2.4G2; BD Biosciences) for 15 min. Extracellular staining was performed for 30 min on ice using: CD4-BV521 (RM4-5; BioLegend, San Diego, CA, USA), CD45-BV510 (30-F11; BioLegend), CD3-APC (17.A2, BioLegend), CD25-PE-Cy7 (PC61; BioLegend), CD8-PerCPCy5.5 (53-6.7; BioLegend), B220 (RA3-6B2; BD Biosciences), CD11b-PE-Cy7 (M1/70; BioLegend), Ly6C-PE (HK1.4; BioLegend), Gr1-APC-Cy7 (RB6-8C5, BioLegend), IA/IE-BV421 (M5/114.15.2, BioLegend), F4/80-FITC (BM8, BioLegend), CD11c-PerCPCy5.5 (N418, BioLegend).

After staining for extracellular proteins, cells were fixed in 4% PFA and permeabilised using 0.1% saponin buffer containing 0.1% bovine serum albumin. Intracellular cytokines were detected with IFNγ-BV421 (XMG 1.2, BioLegend), IL-10-PE (54902, BD Bioscience), and IL-17A-AF647 (TC11-18H10, BioLegend).

Flow cytometry was performed on a BD FACS Canto II (BD Biosciences) and analysed using FlowJo software version 10.6 (Treestar Inc., Ashland, OR, USA).

Tissue processing for histology

Following CO_2 euthanasia and perfusion with phosphate-buffered saline (PBS), spinal cords were fixed in 4% paraformaldehyde overnight at 4 °C. Tissue was cryoprotected in 15% sucrose, followed by 30% sucrose overnight at 4°C or until the tissue sank to the bottom of the tube. The sections were embedded in Cryomatrix embedding resin (Thermo Fisher Scientific), snap-frozen in isopentane on dry-ice, and stored at −80 °C. Three transverse 20 μm sections were taken per animal from descending regions of the cervical spinal cord, were cut using a Leica CM3050 S cryostat microtome (Leica Biosystems), mounted on Superfrost Plus slides (Thermo Fisher Scientific) and stored at −80 °C. Prior to staining, slides were warmed at room temperature for 15–20 min, and Cryomatrix embedding medium was removed by immersing the slides in ddH$_2$O for 5 min.

Black Gold II staining and analysis

Black Gold II Myelin staining (Sigma-Aldrich) was performed as described by the manufacturer. During myelin analysis, all samples were blinded from the assessor. To quantify myelin, the percentage of myelin coverage in the region of interest (ROI) was calculated. Using ImageJ, images of Black Gold II-stained sections were converted to an RGB stack, and the green filter was selected. In the selected ROI (Supplementary figure 1), the colour was inverted, and a threshold was set based on healthy controls. The white matter area was selected, and the percentage area of myelin stain was measured. The lesion area was determined by the manual section of lesions in the white matter and presented as a percentage of total white matter. From this, the number of lesions was counted. The analysis was carried out on 2 or 3 sections per animal, and these sections were averaged to generate a mean value for each animal.

Transmission electron microscopy

Mice assigned for transmission electron microscopy (TEM) were euthanised by lethal administration of sodium pentobarbital (ProVet). The mice were transcardially perfused for approximately 10 min using a prewash (5% heparin sodium salt in PBS containing 145 nM NaCl, 22 mM Na$_2$HPO$_4$, 1.8 mM NaH$_2$PO$_4$, pH 7.4) followed by a primary Karnovsky fixative (0.1 M (CH$_3$)$_2$AsO$_2$Na·3H$_2$O, 4% PFA, 0.25% glutaraldehyde, pH 7.4). For the spinal cord: the whole spinal column was cut out, and the spinal cord was dissected out. The spinal cord was placed in a secondary Karnovsky fixative (0.1 M (CH$_3$)$_2$AsO$_2$Na·3H$_2$O, 4% PFA,

2.5% glutaraldehyde, pH 7.4) and left at 4 °C overnight while gently rocking. A 1-mm³ section of the cervical spinal cord white matter region was cut. For the brain, the entire brain was gently removed, and a 1-mm thick coronal section caudal to bregma was isolated using a brain matrix block. The midline sector of the corpus callosum from each coronal brain section was trimmed under a dissecting microscope. The trimmed samples were washed in sodium cacodylate buffer (0.1 M $(CH_3)_2AsO_2Na{\cdot}3H_2O$, pH 7.4), and transferred into osmium tetroxide solution (1% OsO_4) for 2.5 h. The samples underwent tertiary fixation in 1% uranyl acetate for 2 h and were dehydrated through increasing concentrations of ethanol. The samples were embedded in epoxy resin (#45359-1EA-F, Sigma, US) for polymerisation at 60 °C for 48 h.

Sectioning and imaging

Semi-thin sections were taken using a glass knife and stained with toluidine blue to determine the correct region and orientation. Transverse ultrathin sections (90–60 nm) were cut with a diamond knife (DiATOME, 45 degrees, 3.5–4.4 mm), and the samples were stained with lead citrate and uranyl acetate. Images were taken on a Philips CM100 TEM at the Otago Micro and Nanoscale Imaging unit located at the University of Otago or a JOEL 2010 TEM at the MacDiarmid Institute of Victoria University of Wellington using GATAN software.

Myelin assessment

For both EAE and cuprizone experiments, TEM images were blinded from the assessor. For g-ratio assessment, the outer and inner axonal diameter lengths were measured for each axon across the whole image for EAE samples, and in a specific ROI (9736 × 8095 nm) for cuprizone samples. Only complete axons were analysed. The g-ratios were calculated by dividing the inner axonal diameter by the outer axonal diameter. The g-ratio analysis was carried out on at least 5 images per animal.

Statistical analyses

All graphs and statistical analyses were generated using GraphPad Prism 8 (GraphPad Software Inc., La Jolla, CA USA). Comparisons between two groups were performed using the non-parametric Mann–Whitney test. For comparison of more than two groups, 1-way or 2-way analysis of variance (ANOVA) was used with the recommended multiple comparison tests as indicated in the figure legends. Non-parametric analyses of more than two groups were performed with a Kruskal–Wallis test. Differences of $P < 0.05$ were considered significant.

CONFLICTS OF INTEREST

The author(s) declared the following potential conflicts of interest with respect to the research, authorship and/or publication of this article: Anne Camille La Flamme, Bronwyn M. Kivell and Thomas Prisinzano are inventors on patent applications that relate to this work and have been licensed to Rekover Therapeutics Ltd. ACL, BK and TP hold equity in Rekover Therapeutics Ltd. The authors declare no other financial interests.

AUTHOR CONTRIBUTIONS

Lisa Denny: Conceptualization; Data curation; Formal analysis; Investigation; Writing-original draft. **Afnan Al Abadey:** Data curation; Investigation; Methodology; Writing-original draft. **Katharina Robichon:** Conceptualization; Data curation; Investigation; Methodology; Writing-review & editing. **Nikki Templeton:** Data curation; Investigation; Methodology. **Thomas E Prisinzano:** Conceptualization; Methodology; Resources; Writing-review & editing. **Bronwyn M Kivell:** Conceptualization; Formal analysis; Funding acquisition; Supervision; Writing-review & editing. **Anne Camille La Flamme:** Conceptualization; Data curation; Funding acquisition; Supervision; Writing-review & editing.

ETHICAL APPROVAL

The Victoria University of Wellington Animal Ethics Committee approved all experimental procedures used in this study (2014-R23, 24383, and 25295).

DATA AVAILABILITY STATEMENT

The data sets supporting the conclusions of this article are included within the article (and its Supplementary figures).

REFERENCES

1. Kesselring J, Beer S. Symptomatic therapy and neurorehabilitation in multiple sclerosis. *Lancet Neurol* 2005; **4**: 643–652.
2. Frischer JM, Weigand SD, Guo Y *et al*. Clinical and pathological insights into the dynamic nature of the white matter multiple sclerosis plaque. *Annal Neurol* 2015; **78**: 710–721.

3. Machado-Santos J, Saji E, Tröscher AR *et al*. The compartmentalized inflammatory response in the multiple sclerosis brain is composed of tissue-resident CD8^{+} T lymphocytes and B cells. *Brainy* 2018; **141**: 2066–2082.

4. Podbielska M, Banik NL, Kurowska E, Hogan EL. Myelin recovery in multiple sclerosis: the challenge of remyelination. *Brain Sci* 2013; **3**: 1282–1324.

5. Simonin F, Gavériaux-Ruff C, Befort K *et al*. κ-Opioid receptor in humans: cDNA and genomic cloning, chromosomal assignment, functional expression, pharmacology, and expression pattern in the central nervous system. *PNAS* 1995; **92**: 7006.

6. Peckys D, Landwehrmeyer GB. Expression of *mu*, *kappa*, and *delta* opioid receptor messenger RNA in the human CNS: a [33]P *in situ* hybridization study. *Neuroscience* 1999; **88**: 1093–1135.

7. Peng J, Sarkar S, Chang SL. Opioid receptor expression in human brain and peripheral tissues using absolute quantitative real-time RT-PCR. *Drug Alcohol Depend* 2012; **124**: 223–228.

8. Wittert G, Hope P, Pyle D. Tissue distribution of opioid receptor gene expression in the rat. *Biochem and Biophys Res Commun* 1996; **218**: 877–881.

9. Bagnol D, Mansour A, Akil H, Watson SJ. Cellular localization and distribution of the cloned *mu* and *kappa* opioid receptors in rat gastrointestinal tract. *Neuroscience* 1997; **81**: 579–591.

10. Alicea C, Belkowski SM, Sliker JK *et al*. Characterization of κ-opioid receptor transcripts expressed by T cells and macrophages. *J Neuroimmunol* 1998; **91**: 55–62.

11. Du C, Duan Y, Wei W *et al*. *Kappa* opioid receptor activation alleviates experimental autoimmune encephalomyelitis and promotes oligodendrocyte-mediated remyelination. *Nat Commun* 2016; **7**: 11120.

12. Walsh SL, Strain EC, Abreu ME, Bigelow GE. Enadoline, a selective *kappa* opioid agonist: comparison with butorphanol and hydromorphone in humans. *Psychopharmacology* 2001; **157**: 151–162.

13. Kivell B, Prisinzano TE. *Kappa* opioids and the modulation of pain. *Psychopharmacology* 2010; **210**: 109–119.

14. Kaski SW, White AN, Gross JD *et al*. Preclinical testing of nalfurafine as an opioid-sparing adjuvant that potentiates analgesia by the *Mu* Opioid receptor-targeting agonist morphine. *J Pharmacol Exp Ther* 2019; **371**: 487–499.

15. Nagase H, Hayakawa J, Kawamura K *et al*. Discovery of a structurally novel opioid *kappa*-agonist derived from 4,5-epoxymorphinan. *Chem Pharm Bull (Tokyo)* 1998; **46**: 366–369.

16. Schattauer SS, Kuhar JR, Song A, Chavkin C. Nalfurafine is a G-protein biased agonist having significantly greater bias at the human than rodent form of the *kappa* opioid receptor. *Cell Signal* 2017; **32**: 59–65.

17. Kozono H, Yoshitani H, Nakano R. Post-marketing surveillance study of the safety and efficacy of nalfurafine hydrochloride (Remitch®) capsules 2.5 μg) in 3,762 hemodialysis patients with intractable pruritus. *Int J Nephrol Renovasc Dis* 2018; **11**: 9–24.

18. Mori T, Nomura M, Nagase H *et al*. Effects of a newly synthesized κ-opioid receptor agonist, TRK-820, on the discriminative stimulus and rewarding effects of cocaine in rats. *Psychopharmacology* 2002; **161**: 17–22.

19. EAE Induction by Active Immunization in C57BL/6 Mice 2019. https://hookelabs.com/protocols/eaeAI_C57BL6.html

20. Eisenstein TK. The role of opioid receptors in immune system function. *Front Immunol* 2019; **10**: 2904.

21. Mei F, Mayoral SR, Nobuta H *et al*. Identification of the *Kappa*-opioid receptor as a therapeutic target for oligodendrocyte remyelination. *J Neurosci* 2016; **36**: 7925–7935.

22. Portoghese PS, Nagase H, Lipkowski AW, Larson DL, Takemori AE. Binaltorphimine-related bivalent ligands and their *kappa* opioid receptor antagonist selectivity. *J Med Chem* 1988; **31**: 836–841.

23. Munro TA, Berry LM, Van't Veer A *et al*. Long-acting κ opioid antagonists nor-BNI, GNTI and JDTic: pharmacokinetics in mice and lipophilicity. *BMC Pharmacol* 2012; **12**: 5.

24. Simonson B, Morani AS, Ewald AWM *et al*. Pharmacology and anti-addiction effects of the novel κ opioid receptor agonist Mesyl Sal B, a potent and long-acting analogue of salvinorin A. *Br J Pharmacol* 2015; **172**: 515–531.

25. Chavkin C, Cohen JH, Land BB. Repeated administration of norbinaltorphimine produces cumulative *Kappa* opioid receptor inactivation. *Front Pharmacol* 2019; **10**: 88.

26. Endoh T, Matsuura H, Tanaka C, Nagase H. Nor-binaltorphimine: a potent and selective *kappa*-opioid receptor antagonist with long-lasting activity *in vivo*. *Arch Int Pharmacodyn Ther* 1992; **316**: 30–42.

27. Bruchas MR, Yang T, Schreiber S *et al*. Long-acting *kappa* opioid antagonists disrupt receptor signaling and produce noncompetitive effects by activating c-Jun N-terminal kinase. *J Biol Chem* 2007; **282**: 29803–29811.

28. Cunniffe N, Coles A. Promoting remyelination in multiple sclerosis. *J Neurol* 2019. https://doi.org/10.1007/s00415-019-09421-x. Epub ahead of print.

29. Franklin RJM, Goldman SA. Glia disease and repair-remyelination. *Cold Spring Harb Perspect Biol* 2015; **7**: a020594.

30. Constantinescu CS, Farooqi N, O'Brien K, Gran B. Experimental autoimmune encephalomyelitis (EAE) as a model for multiple sclerosis (MS). *Br J Pharmacol* 2011; **164**: 1079–1106.

31. Tangherlini G, Kalinin DV, Schepmann D *et al*. Development of novel quinoxaline-based κ-opioid receptor agonists for the treatment of neuroinflammation. *J Med Chem* 2018; **62**: 893–907.

32. Rangachari M, Kuchroo VK. Using EAE to better understand principles of immune function and autoimmune pathology. *J Autoimmun* 2013; **45**: 31–39.

33. Al-Hashimi M, Scott SWM, Thompson JP, Lambert DG. Opioids and immune modulation: more questions than answers. *Br J Anaesth* 2013; **111**: 80–88.

34. Liang X, Liu R, Chen C, Ji F, Li T. Opioid system modulates the immune function: a review. *Transl Perioper Pain Med* 2016; **1**: 5–13.

35. Legroux L, Arbour N. Multiple sclerosis and T Lymphocytes: an entangled story. *J Neuroimmune Pharmacol* 2015; **10**: 528–546.

36. Sun D, Whitaker JN, Huang Z *et al*. Myelin antigen-specific CD8^{+} T cells are encephalitogenic and produce severe disease in C57BL/6 mice. *J Immunol* 2001; **166**: 7579–7587.

37. Arellano G, Ottum PA, Reyes LI, Burgos PI, Naves R. Stage-specific role of interferon-*gamma* in experimental autoimmune encephalomyelitis and multiple sclerosis. *Front Immunol* 2015; **6**: 492.

38. Annibali V, Ristori G, Angelini DF *et al*. CD161^high^CD8^+^ T cells bear pathogenetic potential in multiple sclerosis. *Brain* 2011; **134**: 542–554.

39. McGinley AM, Sutton CE, Edwards SC *et al*. Interleukin-17A serves a priming role in autoimmunity by recruiting IL-1β-producing myeloid cells that promote pathogenic T cells. *Immunity* 2020; **52**: 342–356.

40. Becher B, Segal BM. Th17 cytokines in autoimmune neuro-inflammation. *Curr Opin Immunol* 2011; **23**: 707–712.

41. Hedegaard CJ, Krakauer M, Bendtzen K, Lund H, Sellebjerg F, Nielsen CH. T helper cell type 1 (Th1), Th2 and Th17 responses to myelin basic protein and disease activity in multiple sclerosis. *Immunology* 2008; **125**: 161–169.

42. Zhang X, Koldzic DN, Izikson L *et al*. IL-10 is involved in the suppression of experimental autoimmune encephalomyelitis by CD25^+^CD4^+^ regulatory T cells. *Int Immunol* 2004; **16**: 249–256.

43. Sinha S, Boyden AW, Itani FR, Crawford MP, Karandikar NJ. CD8^+^ T-cells as immune regulators of multiple sclerosis. *Front Immunol* 2015; **6**: 619.

44. West KL, Kelm ND, Carson RP, Does MD. Quantitative analysis of mouse corpus callosum from electron microscopy images. *Data Brief* 2015; **5**: 124–128.

45. Piscopo DM, Weible AP, Rothbart MK, Posner MI, Niell CM. Changes in white matter in mice resulting from low-frequency brain stimulation. *Proc Natl Acad Sci USA* 2018; **115**: e6339–e6346.

Supporting Information

Additional supporting information may be found online in the Supporting Information section at the end of the article.